Presence of Metallic Fe Nanoclusters in α-$(Al,Fe)_2O_3$ Solid Solutions

Valdirene G. de Resende,*,†,‡ Anne Cordier,‡ Eddy De Grave,† Christophe Laurent,‡ Sigrid G. Eeckhout,§ Gabriele Giuli,|| Alain Peigney,‡ Geraldo M. da Costa,⊥ and Robert E. Vandenberghe†

Department of Subatomic and Radiation Physics, University of Ghent, 86 Proeftuinstraat, B-9000 Gent, Belgium, CIRIMAT, CNRS/UPS/INPT, LCMIE, Université Paul-Sabatier, Bât. 2R1, 118 route de Narbonne, F-31062 Toulouse cedex 9, France, European Synchrotron Radiation Facility, 6 rue J. Horowitz, BP220, F-38043 Grenoble, France, Dipartimento di Scienze della Terra and INFM, Università di Camerino, Via Gentile III da Varano, 62032 Camerino, Italy, and Chemistry Department, Federal University of Ouro Preto, 35400-000, Ouro Preto (MG), Brazil

Powders of α-$(Al_{1-x}Fe_x)_2O_3$ solid solutions prepared by the calcination in air of the corresponding γ-$(Al_{1-x}Fe_x)_2O_3$ powders were studied by several techniques including X-ray diffraction, field-emission-gun scanning electron microscopy, transmission Mössbauer spectroscopy, integral low-energy electron Mössbauer spectroscopy (ILEEMS), and Fe K-edge X-ray absorption near-edge structure (XANES) measurements. The asymmetry of the characteristic Mössbauer doublet representing Fe^{3+} ions substituting for Al^{3+} ions in the corundum lattice of α-$(Al_{1-x}Fe_x)_2O_3$ solid solutions was resolved and explained for the first time by using two additional subspectra, i.e., a broad second doublet characteristic of a very distorted octahedral site for Fe^{3+} and a singlet attributable to α-Fe, suggesting the presence of metallic iron nanoclusters consisting of only a few number of atoms within the solid solution grains. ILEEMS studies showed that the Fe nanoclusters are evenly distributed among the surface layers and the cores of the grains. Fe K-edge XANES measurements further confirmed the occurrence of metallic iron. The proportion of Fe nanoclusters increases when the total iron content is decreased, as does the proportion of distorted octahedral site, suggesting that they are located around the iron nanoclusters. The formation of the metallic Fe nanoclusters in the α-$(Al_{1-x}Fe_x)_2O_3$ grains is thought to be a consequence of the γ → α phase transition which implies structural rearrangement on both the cationic and anionic sublattices.

Introduction

Alumina, α-Al_2O_3, possess the corundum structure which is based on a hexagonal close-packed (hcp) array of oxygen anions, where $^2/_3$ of octahedral (O_h) interstices are occupied by aluminum cations in a regular way.[1] α-$(Al_{1-x}Fe_x)_2O_3$ solid solutions have been studied for decades usually in order to determine the solubility limit of hematite (α-Fe_2O_3) into α-Al_2O_3[2−8] but also as precursor materials for the formation of Fe−Al_2O_3[9,10] and carbon nanotube−Fe−Al_2O_3[11,12] nanocomposite powders by reduction in H_2 and H_2−CH_4, respectively. Several values have been reported for the solubility limit, in the range of 5−15 mol % (corresponding to 15 cat % of Fe^{3+} ions substituting for Al^{3+} ions in the corundum lattice of alumina). It appears that this strongly depends on the synthesis route. In particular, several methods permit the formation of solid solutions between the metastable sesquioxides of iron (γ-Fe_2O_3) and aluminum (γ-Al_2O_3, δ-Al_2O_3, η-Al_2O_3, and θ-Al_2O_3). The structure of all these metastable oxides is related to that of spinel ($MgAl_2O_4$), owing to the ability of both Fe^{3+} and Al^{3+} ions to occupy tetrahedral (T_d) sites. The stoichiometry can be formally described by the formula $Fe[Fe_{5/3}()_{1/3}]O_4$ and $Al[Al_{5/3}()_{1/3}]O_4$ with the brackets indicating those species occupying the O_h sites. It is well-known[3,4,6−8] that an appropriate heat-treatment of such metastable γ-$(Al_{1-x}Fe_x)_2O_3$ solid solutions can produce α-solid solutions without any phase partitioning into an alumina-rich corundum phase (α_1) and a hematite-rich corundum phase (α_2).

Mössbauer spectroscopy was used as a unique characterization tool in the course of these investigations. Interestingly, several studies where the solid solutions were prepared using chloride,[5] sol−gel,[9] oxalate,[10] and combustion[8] reported that the characteristic doublet representing Fe^{3+} ions substituting for Al^{3+} ions in the corundum lattice more or less clearly exhibited a significant asymmetry, which was never satisfactorily accounted for. Several authors[9,10] applied an extended velocity scale, making the asymmetry less enhanced and consequently thought to be insignificant. The explanations proposed by Brown et al.[5] and Cordier et al.[8] will be discussed later in the text.

With the aim to shed some light into that matter, α-$(Al_{1-x}Fe_x)_2O_3$ powders were prepared by an oxinate route different from all those used earlier. The present paper reports a major interdisciplinary research project concerning some remarkable features, believed to be related to the γ → α transition, involving for the first time the presence of metallic Fe nanoclusters within α-$(Al_{1-x}Fe_x)_2O_3$ grains.

Experimental Section

γ-$(Al_{1-x}Fe_x)_2O_3$ powders (containing 2, 5, 7, and 10 cat % Fe) with a high specific surface area (over 200 m^2/g) were

* To whom correspondence should be addressed. Fax: +32-(0)9-264-6697. E-mail: Valdirene.Gonzaga@Ugent.be.
† University of Ghent.
‡ Université Paul-Sabatier.
§ European Synchrotron Radiation Facility.
|| Università di Camerino.
⊥ Federal University of Ouro Preto.

10.1021/jp8032098

prepared from the decomposition of the mixed oxinates. The details of the preparation of the γ-$(Al_{1-x}Fe_x)_2O_3$ powders will be reported elsewhere. To determine the $\gamma \rightarrow \alpha$ transition temperatures, differential thermal analyses (DTA) were carried out (Du Pont SDT 2960) on small samples of each powder. The DTA curves were recorded in the range 25−1300 °C, using a flow of synthetic air (100 mL/min) and a heating rate of 10 °C/min. On the basis of the DTA results, the γ-$(Al_{1-x}Fe_x)_2O_3$ powders were appropriately heat-treated in air in order to obtain the respective α-phases. The resulting α-$(Al_{1-x}Fe_x)_2O_3$ powders were code-named as aAFY in which Y stands for the Fe content expressed as cat %.

Powder X-ray diffraction (XRD) patterns were recorded in the range 20−70° (2θ) using a Seifert 3003 TT diffractometer equipped with a Cu Kα radiation tube. The cell parameters were calculated by the Rietveld method using the "Fullprof" software.[13] The specific surface area of the aAFY powders was measured by the Brunauer−Emmett−Teller (BET) method (Micrometrics Flow Sorb II 2300) using nitrogen adsorption at liquid nitrogen temperature. This instrument gives a value from one adsorbate pressure and requires calibration. The reproducibility of the results is in the ±3% range. The powders were further examined by field-emission-gun SEM (FEG-SEM, JEOL JSM 6700F). Mössbauer spectra (MS) at 295 K and at 4.2 K were collected with a spectrometer operating at constant acceleration mode with triangular reference signal. ^{57}Co(Rh) source was used, but isomer shift values quoted hereafter are referenced with respect to α-Fe at 295 K. The absorbers had a thickness of at most approximately 7 mg of Fe per cm^2. Velocity calibration was achieved by recording spectra of an α-Fe foil or a standard thin α-Fe_2O_3 absorber at room temperature. For the latter the inner line width was typically 0.27 mm/s. A selected sample was studied by integral low-energy electron Mössbauer spectroscopy (ILEEMS). ILEEMS is a variant of conventional transmission Mössbauer spectroscopy in which the resonant low-energy (~10 eV) electrons are counted.[14] These electrons are produced by after effects in the decay process of the excited probe Mössbauer nuclei in the absorber following resonant absorption of incident γ-quanta. Combined with transmission Mössbauer spectrometry, the results of ILEEMS yield semiquantitative information about the chemical state of a thin surface layer (5−10 nm) of the material from which the majority of the detected low-energy electrons originate.

Fe K-edge XANES spectra were recorded at room temperature at the European Synchrotron Radiation Facility on the undulator beamline ID26[15,16] operating at 6 GeV and 200 mA in 2*1/3 filling mode. A fixed-exit Si (311) double-crystal monochromator was used. The energy was calibrated by defining the first derivative peak of a metallic Fe reference foil to be 7112.0 eV. Two Si mirrors were used for the harmonics rejection of the incident X-ray beam. XANES data were recorded in quick-scan mode by simultaneously scanning the monochromator angle and the undulator gap with a typical energy step of 0.2 eV in the pre-edge region. The spectra were acquired in fluorescence mode, using a Si photodiode. The incident flux was monitored by detecting the X-ray scattering from a thin Kapton foil in the incident beam path. The sample was positioned at 45° with respect to the beam. Experimental X-ray absorption near-edge structure (XANES) spectra were reduced by background subtraction with a linear function and then normalized for atomic absorption on the average absorption coefficient of the spectral region from 7150 to 7250 eV. Pre-edge peak analysis was carried out following the procedure reported in Wilke et al.[17] and Giuli et al.[18] The pre-edge peak was fitted by a sum of pseudo-Voigt functions.

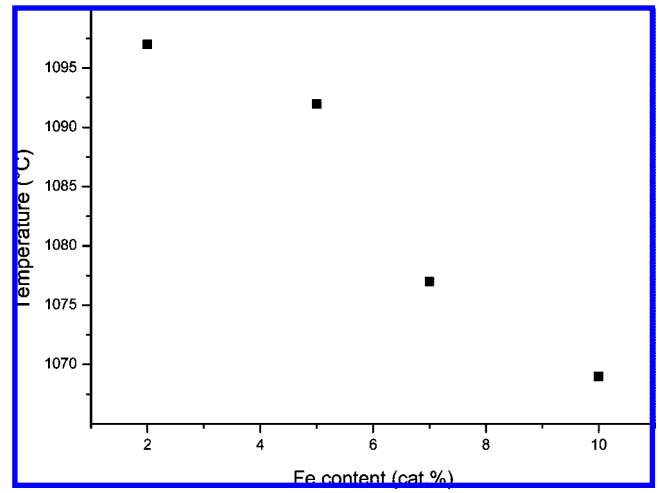

Figure 1. Temperature of the DTA peak assigned to the $\gamma \rightarrow \alpha$ phase transition as a function of the iron content on the $(Al,Fe)_2O_3$ solid solutions.

Results and Discussion

The DTA curves of all four powders exhibit an exothermic peak at a temperature that slightly decreases with increasing Fe content from 1097 °C for 2 cat % to 1069 °C for 10 cat % (Figure 1). This peak is assigned to the $\gamma \rightarrow \alpha$ phase transition, and the observed correlation with Fe substitution is in agreement with earlier results.[4,10] However, the γ-$(Al_{1-x}Fe_x)_2O_3$ samples with 7 and 10 cat % Fe exhibit a second exothermic peak at ~1234 °C, which is, according to the XRD patterns (being presented hereafter), attributable to phase partitioning into an alumina-rich corundum phase (α_1) and a hematite-rich corundum phase (α_2).

On the basis of the above DTA results, the γ-$(Al_{1-x}Fe_x)_2O_3$ powders were calcined at 1120 °C (2 and 5 cat % Fe) or 1100 °C (7 and 10 cat % Fe), in order to obtain the respective α-phases. The samples were heated up to 600 °C at a rate of 300 °C/h and then further heated at a rate of 900 °C/h up to the desired temperatures of 1120 or 1100 °C, respectively. A dwell time at these temperatures of 30 min was applied, and subsequently the products were allowed to cool down to room temperature at furnace rate, thus finally yielding the various aAFY samples.

The XRD patterns of the aAFY samples (Figure 2) show peaks characteristic of well-crystallized corundum solid solution. For aAF10, however, several weak additional lines corresponding to hematite (α-Fe_2O_3) are observed. This indeed implies that for this composition the crystallization of the solid solution into the α phase was followed by some degree of phase partitioning. This result is in agreement with the DTA result as mentioned above. This finding further infers that the solubility limit of hematite into the α-Al_2O_3 structure for the present synthesis route is below 10 mol %. The hexagonal unit-cell parameters a and c of the aAFY samples as obtained from the XRD data were plotted (Figure 3) as a function of the iron content after having corrected the cat % for the fraction of Fe^{3+} cations present in the hematite phase, the latter being determined from the MS (see hereafter). Both a and c increase with increasing iron content, implying that the Fe^{3+} cations, which possess a larger ionic radius as compared to Al^{3+}, are at substitutional sites in the corundum structure. The experimental

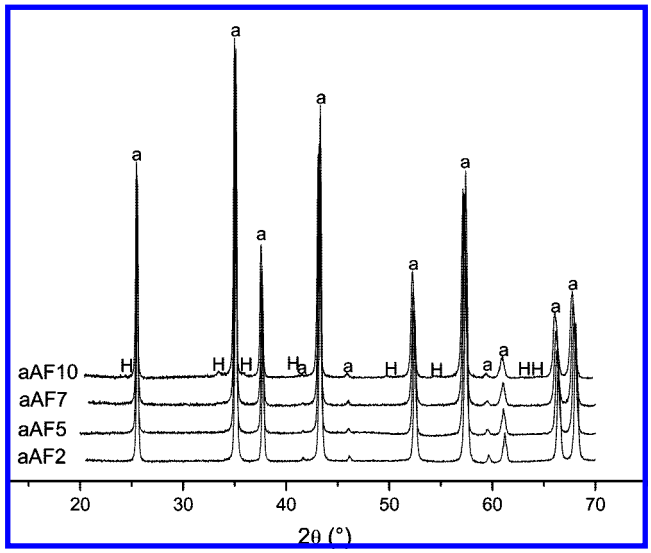

Figure 2. XRD patterns of the powders prepared by calcination in air of the corresponding γ-$(Al_{1-x}Fe_x)_2O_3$ solid solutions. H = hematite; a = alumina.

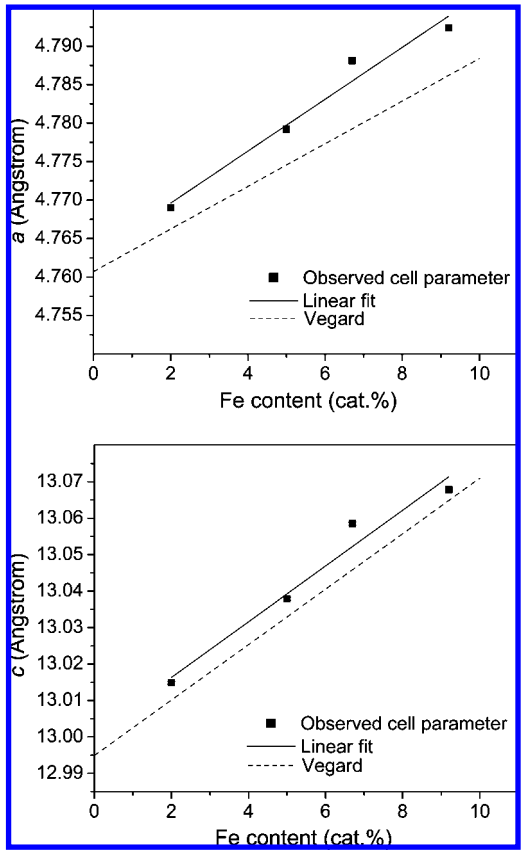

Figure 3. (a) Cell parameter a and (b) cell parameter c, as obtained from the XRD patterns. The black squares correspond to the experimental a and c cell parameters. The errors for the experimental points are smaller than their size (black squares). The solid line is a linear fit through the experimental points, and the dashed line represents the Végard's law.

a and c data are compared with the values predicted by Végard's law (dashed straight lines in Figure 3), using for the latter the lattice parameters of α-Al_2O_3 as reported on the PDF card (83−2080) and those of a α-Fe_2O_3 powder prepared by the oxinate decomposition route as given by da Costa et al.[19] It is clear that both unit cell parameters for the present aAFY samples deviate from the corresponding Végard values. These deviations

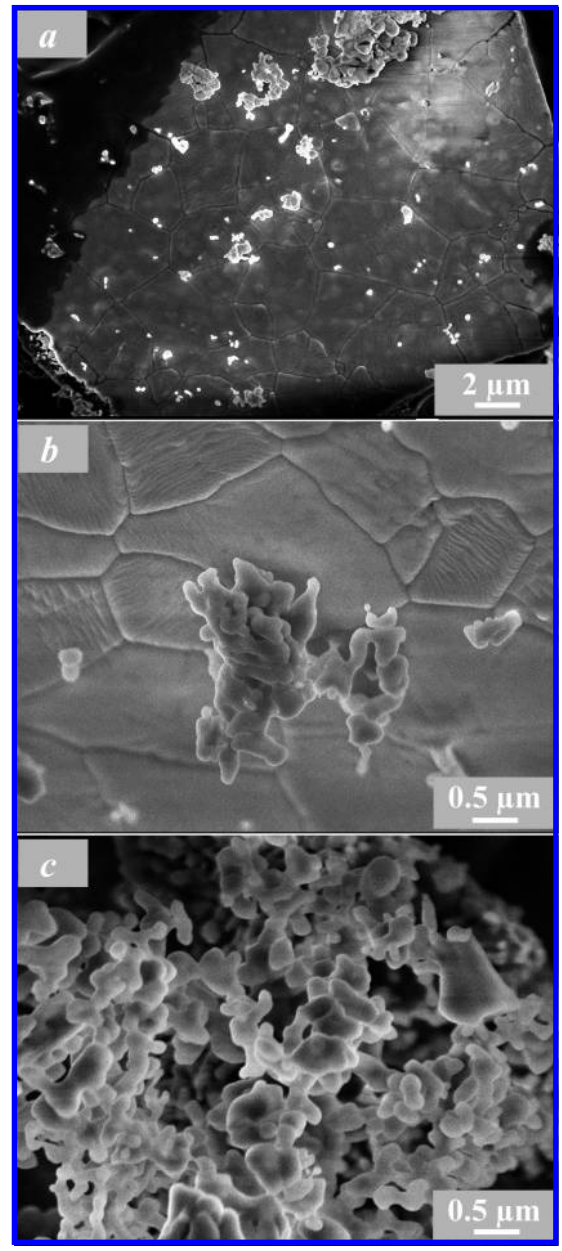

Figure 4. FEG-SEM images of the aAF5 powder.

may be due to the presence of strain in the lattice which is eventually removed by the partial phase partitioning in those samples with higher Fe contents. Another possible explanation is the formation of metallic iron clusters, which will be presented and discussed in the following MS section.

FEG-SEM images of the powders reveal that they are made up of 2−5 μm grains assembled into tabularlike aggregates (parts a and b of Figure 4). However, the observation of smaller entities and of side-views of the tabular-grains reveals the so-called vermicular microsctructure with much looser aggregates made up of 0.2−0.5 μm primary grains or crystallites (Figure 4c). The BET specific surface area of the aAFY powders was found to be about 5 m^2/g, much lower than for the parent γ-$(Al_{1-x}Fe_x)_2O_3$ powders (over 200 m^2/g). This results from the strong structural rearrangement occurring on both the cationic and anionic sublattices that has taken place during the transformation process and from a high degree of sintering.

MS (Figure 5) were recorded at 295 K for the four aAFY powders described above. In view of the results thereof, two additional compositions were prepared in the same manner and

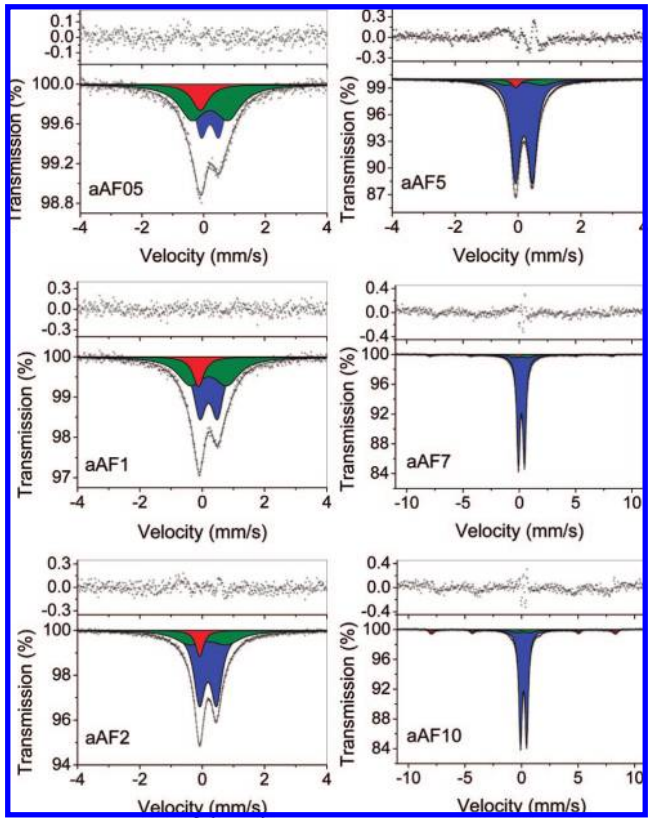

Figure 5. Mössbauer spectra of the α-$(Al_{1-x}Fe_x)_2O_3$ samples measured at room temperature and the respective spectral fitting residuals. The doublet D2 with large quadrupole splitting is shaded in olive while the singlet Sg due to Fe clusters is shaded in red and the doublet D1 with smaller quadrupole splitting is shaded in blue. The residuals are shown above each spectrum.

characterized by their Mössbauer spectra. These two additional samples contained 0.5 and 1 cat % Fe (aAF05 and aAF1, respectively). The spectra were collected either over a broad velocity range of approximately ±11 mm/s (samples aAF7, aAF10) or using a narrower scale of ±4 mm/s (aAF05, aAF1, aAF2, aAF5). In the MS for aAF2 and aAF5 only a single doublet appears, while for aAF7 and aAF10 clearly a weak sextet in addition to a dominant doublet is recognized. Preliminary fits with superpositions of a Lorentzian-shaped sextet and a doublet yielded values for the hyperfine parameters of the sextet as listed in Table 1 for subspectrum S1. These values, in particular those for the quadrupole shift $2\varepsilon_Q$, are characteristic of α-Fe_2O_3. The rather low value for the hyperfine field B_{hf} (49.8 vs 51.7 T for pure bulk hematite) indicates small-particle size and/or a significant Al-for-Fe substitution for this α-Fe_2O_3 phase.[19] Hence, the MS confirm the earlier mentioned phase partition in the α-$(Al_{1-x}Fe_x)_2O_3$ solid solutions for aAF7 and aAF10.

The smaller velocity range MS show a broadened doublet with significant asymmetry in peak depths for all four samples, however, gradually lowering with increasing Fe substitution. The asymmetry might be explained by a texture effect resulting from a preferential orientation of the particles with regard to the absorber plane. According to the FEG-SEM images (Figure 4), the powders are indeed composed of large platelike particles. It is not unlikely that such morphology induces a texture that appears in the MS as an asymmetric doublet. To verify this point, MS have been measured for aAF2 and aAF5 with the absorber planes under an angle of ∼54° with respect to the incident γ-rays. This angle is called "the magic-angle" and has the effect of removing the asymmetry if the latter is due to texture.[20] The procedure of Greneche and Varret[21] was followed (see Supporting Information, Figure S1); however, identical asymmetric line shapes were present in these magic-angle MS, hence ruling out a texture effect.

Another explanation for the asymmetry of the doublet was proposed by Cordier et al.[8] For powders with 10 cat % Fe-for-Al substitution, the presence of a weak doublet ($\Delta E_Q \approx 1.3$ mm/s) was reported in addition to the predominant Fe^{3+} doublet with quadrupole splitting $\Delta E_Q \approx 0.54$ mm/s, which indeed reproduced the slight asymmetry reasonably well. The authors ascribed this weak doublet to a strongly distorted octahedral Fe^{3+} site in the α-alumina structure.

Attempts to fit the broad doublet component in the present spectra using superpositions of two symmetric doublets failed in the sense that inconsistent parameter values were obtained and that the adjusted line shapes showed small, but significant misfits with respect to the experimental data, in particular for the lower Fe-for-Al substitutions (see Supporting Information, Figure S2). These misfits seemed to indicate that, in addition to the two doublets, a singlet component is present as well. Thus, each of the asymmetric doublets was fitted with a superposition of a major doublet D1, a minor doublet D2, and a singlet Sg. The two doublets were described as independent quadrupole splitting distributions, while the singlet was considered as a single Lorentzian line. This model produced excellent fits of the experimental MS (solid lines in Figure 5) with relevant parameters as listed in Table 1. Some restrictions had to be imposed for the iteration procedure to reach convergency with reasonable parameter values. These restrictions are specified in the footnotes to Table 1. The residuals, i.e., the experimental minus the fitted spectra, are shown above each spectrum (Figure 5). It is evident that for the three samples with the highest Fe contents, some remaining residual signal is apparent (see also Supporting Information, Figure S3); however, no misfits are observed in the fitted spectra. The authors believe that these small residual signals are insignificant and are thought to be the result of the imposed restrictions, and therefore they do not change the conclusions of the work. The goodness-of-fit χ^2 for the lowest Fe contents was in the average around 1.2 while for the higher contents it was about twice as high. The line width values of the singlet component increased from ∼0.30 to 0.65 mm/s as the iron content in the samples decreased. For the doublet components, which were fitted using distribution profile, the line widths of the elemental doublets are not mentioned because, as is generally recognized, their values have little relevance.

It is important to stress that the existence of this singlet was confirmed by the MS obtained for a powder equivalent to aAF2 synthesized independently (i.e., in another laboratory) by the same oxinate route, which is identical to the spectrum shown in Figure 5. The actual superposition of the unresolved singlet in the MS makes the apparent quadrupole doublet of the substitutional Fe^{3+} asymmetric in the sense that the negative velocity peak has a slightly but significantly higher resonant absorption than the positive velocity peak.

Brown et al.[5] applied the same three-component model to fit their MS of α-$(Al_{1-x}Fe_x)_2O_3$ solid solutions with iron contents ranging between 2 and 10.5 cat %. They reported hyperfine parameters that are all consistent with the presently obtained values, including for the isomer shift of the singlet, i.e., $\delta \approx 0$ mm/s. These authors[5] considered two possible explanations for the origin of the singlet: (i) the presence of superparamagnetic inclusions of hematite in the alumina grains and (ii) Fe^{3+} cations

TABLE 1: Hyperfine Parameters at Room Temperature for the α-$(Al_{1-x}Fe_x)_2O_3$ Powders[a]

	D1			D2			Sg		S1			
sample	ΔE_Q (mm/s)	δ^b (mm/s)	RA (%)	ΔE_Q (mm/s)	δ^b (mm/s)	RA (%)	δ (mm/s)	RA (%)	B_{hf} (T)	$2\varepsilon_Q$ (mm/s)	δ (mm/s)	RA (%)
aAF05	0.57	0.32	37	1.18	0.32	50	−0.03	13				
aAF1	0.57	0.31	46	1.17	0.31	43	−0.01	11			K	
aAF2	0.54	0.30	63	1.18	0.30	29	0.03	8				
aAF5	0.53	0.30	85	1.18	0.30	12	0.04	3				
aAF7	0.54	0.29	88	1.20	0.29	8	0.05[c]	1	49.8	−0.19	0.35	3
aAF10	0.54	0.29	85	1.20	0.29	7	0.05	0.5	49.8	−0.18	0.37	7.5
aAF2[d]	0.55	0.31	62	1.20	0.31	29	0.03	9				

[a] B_{hf}, hyperfine field at maximum of the distribution (T); $2\varepsilon_Q$, quadrupole shifts (mm/s); ΔE_Q, quadrupole splitting (mm/s); δ, isomer shifts (mm/s); RA, relative spectral areas (%). Estimated errors in the quadrupole splittings/shifts and isomer shifts are 0.02 and 0.01 mm/s, respectively. For the relative spectral areas, the error is about 4% of the actual values. [b] The values of isomer shifts are with reference to metallic iron. The isomer shifts of D1 and D2 were coupled. [c] Fixed parameter. [d] Hyperfine parameters resulting from the ILEEMS spectrum of sample aAF2.

occupying a highly regular site in a spinel impurity. Both explanations were eventually and rightly abandoned by the authors. They further suggested that the singlet corresponds to ferric ions and may be due to a "final remnant of a site" that occurs in the transformation process during the $\gamma \rightarrow \alpha$ phase transition. However, this is not thought to be reasonable because their reported MS parameter ($\delta \approx 0$ mm/s) does not support this.

The appearance of a singlet in the MS with isomer shift slightly different from zero at 295 K, which is characteristic of α-Fe, prompted the idea that extremely small metallic Fe clusters may have formed within the α-$(Al_{1-x}Fe_x)_2O_3$ grains. There seems to be a weak correlation between the isomer shift value and the Fe content; however, considering the experimental error in the data, this conclusion is not sound. That such clusters are indeed extremely small is proven by the observation that even at temperatures as low as 4.2 K their subspectral contribution to the MS remains as a singlet and hence they still are (super-)paramagnetic. This implies, according to a study of Bødker et al.,[22] that the clusters must have dimensions far less than 1 nm.

Moreover, it seems that the weak doublet D2 with large quadrupole splitting $\Delta E_Q \approx 1.19$ mm/s (Table 1), and hence the presence of strongly distorted Fe^{3+} sites in the α-alumina structure, is associated with the occurrence of the iron clusters. The results for the relative spectral areas RA of doublet D2 and singlet Sg (Table 1) indeed indicate that there exists a strong positive correlation between the fraction of total iron that constitutes the metallic clusters on the one hand and the fraction that is attributable to the distorted lattice sites. This finding suggests the idea that in a more or less extended neighborhood of the clusters, the octahedral sites of the α-$(Al_{1-x}Fe_x)_2O_3$ structure are highly distorted so that the iron species situated within this shell of distorted sites exhibit a large quadrupole splitting.

The RA values obtained from the fitted MS of all samples are plotted against the iron content in Figure 6. The proportion of Fe nanoclusters clearly increases when the total iron content is decreased, reaching about 13% for the solid solution with only 0.5 cat % of iron. Furthermore, this plot evidence beyond any doubt that there is a close association between iron clusters and highly distorted octahedral co-ordinations, in the sense that, when the proportion of clusters increases, the fraction of distorted lattice sites increases too, which is plausible if the origin of the distortion is as suggested above.

The formation of metallic iron in the process applied to produce the present α-$(Al_{1-x}Fe_x)_2O_3$ solid solutions being totally unexpected and against any chemical perception, the authors applied Fe K-edge XANES measurements in an attempt to

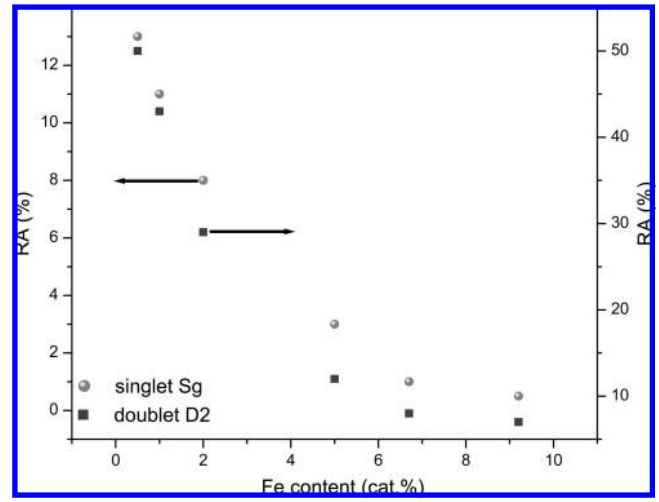

Figure 6. The relative spectral area values of the singlet Sg and the doublet D2 resolved from the Mössbauer spectra as a function of the iron content in the Fe/alumina solid solutions.

confirm the presence of iron in zero valence state. The XANES spectra of aAF2, aAF5, aAF7, aAF10, and of metallic iron are displayed in Figure 7a. The overall shape of the aAF2−aAF10 XANES spectra are comparable, whereas the spectrum of metallic iron is shifted toward lower energy. Close inspection of the energy region before 7120 eV, called the pre-edge region, reveals that the α-$(Al_{1-x}Fe_x)_2O_3$ samples have two distinct pre-edge peak components sitting on the edge slope (Figure 7b). These peaks are assigned to 1s → 3d transitions and used to discriminate the oxidation state and co-ordination number of iron. By calculation of the pre-edge peak centroid and the integrated intensities (Table 2 and Figure 8), these data can be compared with those of the model compounds with known Fe oxidation state and coordination number.[17,18,23,24] For the present α-$(Al_{1-x}Fe_x)_2O_3$ powders, they confirm the presence of ferric iron in 6-fold coordination sites. Furthermore, the absence of a third component in the pre-edge region, which has been assigned to extra transitions related to Fe^{3+}-O_6 clustering,[17,25] shows that no such clustering occurs here. Hence, there are no detectable hematite-like regions in the corundum lattice. The background at the pre-edge region, most clearly observable at the higher-energy side of the pre-edge peaks, increases from aAF5 to aAF2 and further to aAF10 and aAF7. Since the edge for metallic iron occurs at the same position as the pre-edge region of α-$(Al_{1-x}Fe_x)_2O_3$, this feature can be used as a fingerprint for the occurrence of metallic iron in the presently studied samples. By assumption that aAF5 has no metallic iron (lowest background), linear combinations of this spectrum with the one for

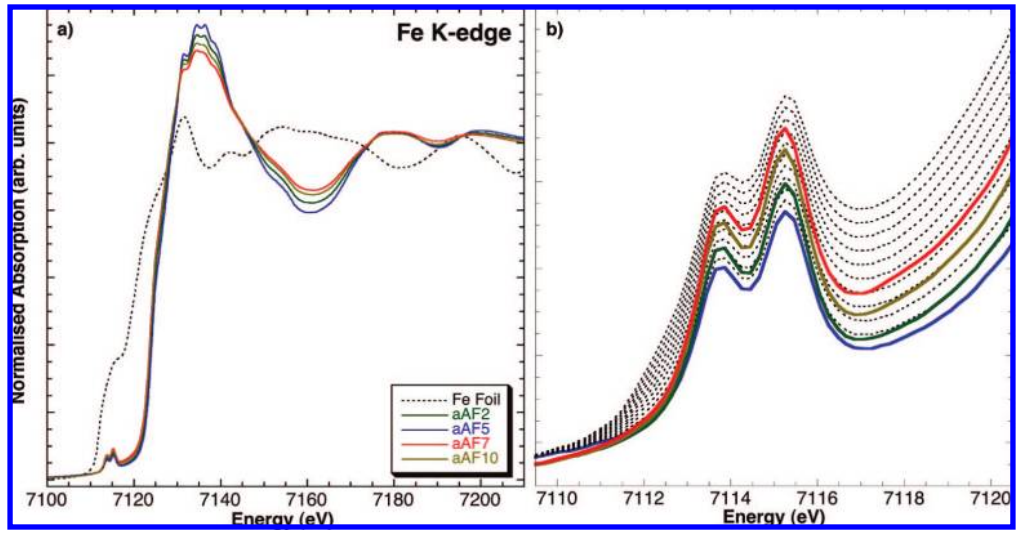

Figure 7. (a) Experimental Fe K-edge XANES spectra of aAF2 (green line), aAF5 (blue line), aAF7 (red line), aAF10 (brown line), and metallic iron (black dotted line). (b) Blow-out of the pre-edge region. The experimental spectra (same symbols as in a) are compared with model spectra (thin dotted lines) obtained by mixing the spectrum of sample aAF5 (lowest background) with the one for Fe metal with weights ranging from 99/1 to 90/10. Note the evident increase of the background intensity at the pre-edge region caused by even small amount of metallic Fe.

TABLE 2: Pre-Edge Peak Features of the Fe K-Edge XANES Spectra

sample name	centroid (eV)[a]	integrated intensity	fit agreement index (%)
aAF2	7114.62	0.136	99.98
aAF5	7114.60	0.109	99.97
aAF7	7114.58	0.148	99.96
aAF10	7114.59	0.133	99.97

[a] Precision and accuracy of the pre-edge peak centroid energy are ± 0.05 and 0.1 eV, respectively.

metallic iron were performed in order to estimate the amount of metallic iron present. The results are shown in Figure 7b. Aside from the observed trend of the background intensity increase at the pre-edge region, increasing amount of metallic iron (when going from aAF5 to aAF2 and further to aAF10 and aAF7) also produces a decrease in the white line intensity and an increase in the intensity of the local minimum around 7160 eV (Figure 7a), as observed in the XANES region.

It is important to note that XANES, in contrast to MS, only allows for a semiquantitative determination of the amount of iron present in metallic state. Therefore, it may not surprise that the fractions of metallic iron in the various samples as suggested by the XANES observations are different from those found from MS (Table 1). However, it is clear that the XANES analyses confirm that zerovalent iron is indeed present in the α-$(Al_{1-x}Fe_x)_2O_3$ grains.

An intriguing question concerns the location of the Fe nanoclusters: are they found exclusively deep inside the grains or rather concentrated in a surface shell? In an attempt to find out, an ILEEMS measurement at 295 K for the aAF2 powder was carried out. The ILEEMS (Figure 9) has the same shape and consists of the same spectral components as the transmission spectrum (Figure 5). The hyperfine parameters of all subspectral components and their relative spectral areas obtained from the ILEEMS are within the error limits identical to the respective values fitted to the transmission MS. This finding is clear evidence that the Fe nanoclusters are evenly distributed among the surface layers and the cores of the α-$(Al_{1-x}Fe_x)_2O_3$ grains. This does not mean that Fe clusters are located on the surface but can be covered with a thin layer of alumina which is sufficient to avoid oxidation of the clusters (see here after).

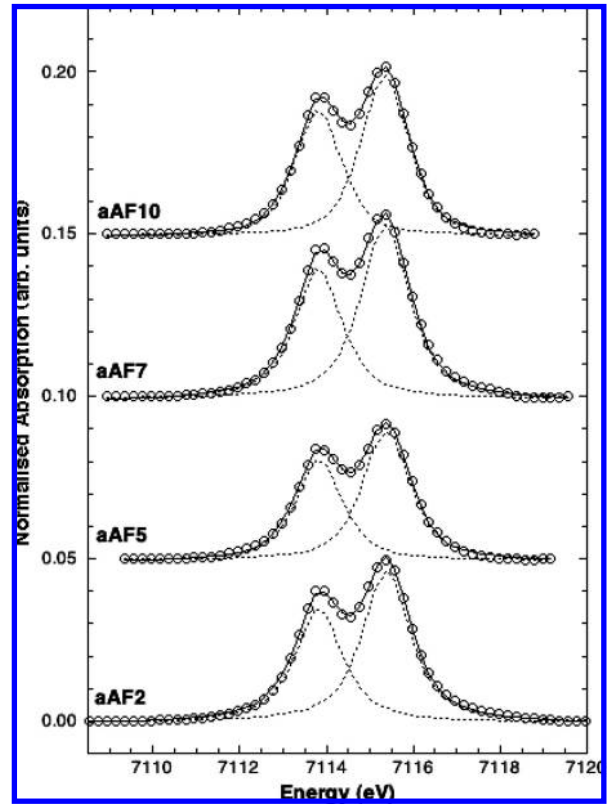

Figure 8. Fit of the pre-edge peaks of samples aAF2, aAF5, aAF7, and aAF10. It is evident the lack of a third feature at about 7117.5 eV, typical of hematite Fe K-edge XANES spectra, which is assigned to a Fe−Fe excitation.[26] The lack of this feature entails the absence of hematite-like domains in the corundum lattice.

It is thus believed that the combined results of MS and XANES have provided convincing arguments to conclude that metallic iron is present in the α-$(Al_{1-x}Fe_x)_2O_3$ grains and that this metallic iron occurs as nanoclusters.

At this point, information that could be interesting concerns the thermal stability of these nanoclusters. For that purpose a batch of powder aAF2 was heated in air at 1120 °C and kept at that temperature during ten hours. After cooling down the sample to room temperature, its measured MS turned out to be

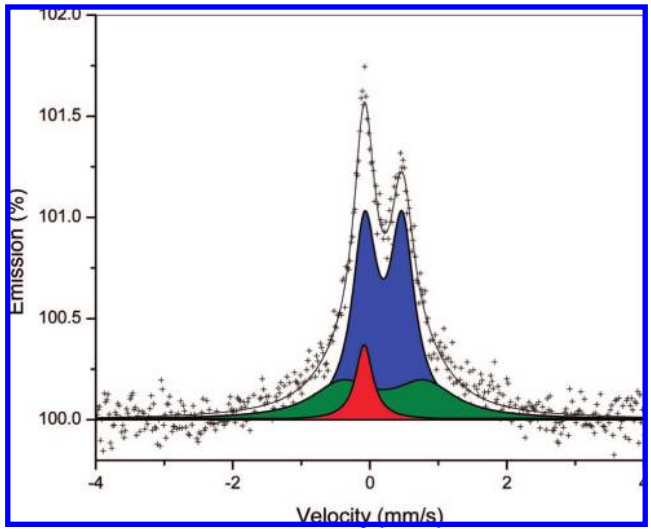

Figure 9. ILEEMS spectrum collected at room temperature for sample aAF2. The weak doublet with large quadrupole splitting is shaded in olive while the singlet due to Fe clusters is shaded in red and the major doublet shaded in blue.

composed of the same components as those observed in the spectrum of the original aAF2 (Figure 5), with roughly equal subspectral areas. It was further experienced that when heating was performed at 1300 °C, also no changes are obvious in the subsequently acquired 295 K MS (see Supporting Information, Figure S4). These results indicate that the iron nanoclusters are extremely stable against heating for long times at relatively high temperatures, which is in agreement with the observations by Brown et al.[5] Moreover, it is interesting to note that, for Fe/Cr−Al_2O_3 and carbon nanotube−Fe−Al_2O_3 powders prepared by reduction in H_2 or H_2−CH_4 of similar corundum solid solutions,[27,28] the oxidation in air of the metal particles (<10 nm in diameter) located inside the Al_2O_3 grains was found to take place at the temperature as high as 1200 °C.

Taking into account that the calcination of the γ-$(Al_{1-x}Fe_x)_2O_3$ powders for the preparation of the α-$(Al_{1-x}Fe_x)_2O_3$ powders was carried out in air, i.e., under oxidizing conditions, it is surprising that metallic Fe nanoclusters have been formed and an explanation for this phenomenon is not evident. It is tentatively suggested that they have their origin in the stress/pressure in the lattice induced by the $\gamma \rightarrow \alpha$ transition. γ-Alumina possess the defective spinel structure, while α-alumina have an hcp arrangement of oxygen anions. Therefore, the phase transition may provoke local stress in the lattice while the structure is rearranging. To support the suggestion that the creation of the nanoclusters is somehow associated with the phase transition, two samples of α-$(Cr_{1-x}Fe_x)_2O_3$ with differents amounts of iron were prepared by decomposition of the mixed-oxalate precursors. The obtained MS at 295 K (not shown) clearly consist of a single narrow Fe^{3+} doublet (line width of ~0.27 mm/s) with no significant asymmetry. As these powders were obtained directly as α-modification and thus no $\gamma \rightarrow \alpha$ phase transition is involved, in contrast to the α-$(Al_{1-x}Fe_x)_2O_3$ powders, it is reasonable to suggest that the formation of metallic Fe nanoclusters in the latter solid solutions is related to the $\gamma \rightarrow \alpha$ transition. What the real driving force may be, however, remains unclear so far.

Conclusions

The aim of this paper was to shed some light into a matter which was reported several times but was never satisfactorily accounted for, regarding the unexpected asymmetry of the characteristic Mössbauer doublet representing Fe^{3+} ions substituting for Al^{3+} ions in the corundum lattice of α-$(Al_{1-x}Fe_x)_2O_3$ solid solutions. The Mössbauer spectra of α-$(Al_{1-x}Fe_x)_2O_3$ powders obtained by the calcination in air of the corresponding γ-$(Al_{1-x}Fe_x)_2O_3$ powders were found to be composed, in addition to the expected Fe^{3+} doublet due to the Fe^{3+} ions substituting for Al^{3+} ions in octahedral sites, of a broad second doublet characteristic of a very distorted octahedral site for Fe^{3+} and a singlet attributable to α-Fe, suggesting for the first time the presence of metallic iron nanoclusters within the solid solution grains. As no magnetic ordering occurs within the nanoclusters at temperatures as low as 4.2 K, it is believed that they consist of only a few number of atoms. ILEEMS studies showed that the Fe nanoclusters are evenly distributed among the surface layers and the cores of the α-$(Al_{1-x}Fe_x)_2O_3$ grains. Fe K-edge XANES measurements allowed ascertainment of the absence of hematite-like domains in the corundum latttice and further confirmed the occurrence of metallic iron. The proportion of Fe nanoclusters increases when the total iron content is decreased, as does the proportion of the very distorted octahedral site, pointing out to a close association between the nanoclusters and distorted site. This could suggest that the distorted octahedral site is located around the iron clusters. The formation of the metallic Fe nanoclusters in the α-$(Al_{1-x}Fe_x)_2O_3$ grains is thought to be a consequence of the $\gamma \rightarrow \alpha$ phase transition which implies structural rearrangement on both the cationic and anionic sublattices.

Acknowledgment. This work was partially funded by the Fund for Scientific Research—Flanders and by the Special Research Fund (BOF, Bijzonder Onderzoeksfonds), UGent (B/06633), Belgium. The authors would like to thank Mr. J. Gurt Santanach (Toulouse) for help with the synthesis of the chromia-based powders and Mr. L. Datas for assistance in FEG-SEM observations, which were performed at TEMSCAN, the "Service Commun de Microscopie Electronique à Transmission", Université Paul Sabatier, Toulouse. One of the authors (G.Md.C.) wants to thank CNPq and Fapemig (Brazil) for financial support. The European Synchrotron Radiation Facility is acknowledged for providing unconditional access to its facilities (ID26).

Supporting Information Available: Figure S1: Mössbauer spectra of sample aAF2 showing the absence of texture effect in the powder. Figure S2: Mössbauer spectra of two of the α-$(Al_{1-x}Fe_x)_2O_3$ samples and the respective spectral fitting residuals showing the misfits. Figure S3: Mössbauer spectrum of sample aAF7 with the remaining residual signal. Figure S4: Mössbauer spectrum of sample aAF2 heated during 10 h at 1300 °C. This material is available free of charge via the Internet at http://pubs.acs.org.

References and Notes

(1) Wolverton, C.; Hass, K. C. *Phys. Rev. B* **2000**, *63*, 024102.
(2) Muan, A.; Gee, C. L. *J. Am. Ceram. Soc.* **1956**, *39*, 207.
(3) Rousset, A.; Pâris, J. *Bull. Soc. Chim. Fr.* **1972**, *10*, 3729.
(4) Bye, G. C.; Simpkin, G. T. *J. Am. Ceram. Soc.* **1974**, *57*, 367.
(5) Brown, I. W. M.; Mackenzie, K. J. D.; Cardile, C. M. *J. Mater. Sci. Lett.* **1987**, *6*, 535.
(6) Escribano, V. S.; Amores, J. M. G.; Finocchio, E.; Daturi, M.; Busca, G. *J. Mater. Chem.* **1995**, *5*, 1943.
(7) Polli, A. D.; Lange, F. F.; Levi, C. G.; Mayer, J. *J. Am. Ceram. Soc.* **1996**, *79*, 1745.
(8) Cordier, A.; Peigney, A.; De Grave, E.; Flahaut, E.; Laurent, Ch. *J. Eur. Ceram. Soc.* **2006**, *26*, 3099.
(9) Verelst, M.; Kannan, K. R.; Subbanna, G. N.; Rao, C. N. R.; Laurent, Ch.; Rousset, A. *J. Mater. Res.* **1992**, *7*, 3072.

(10) Laurent, Ch.; Rousset, A.; Verelst, M.; Kannan, K. R.; Raju, A. R.; Rao, C. N. R. *J. Mater. Chem.* **1993**, *3*, 513.
(11) Peigney, A.; Laurent, Ch.; Dobigeon, F.; Rousset, A. *J. Mater. Res.* **1997**, *12*, 613.
(12) Peigney, A.; Coquay, P.; Flahaut, E.; Vandenberghe, R. E.; De Grave, E.; Laurent, Ch. *J. Phys. Chem. B* **2001**, *105*, 9699.
(13) Rodriguez-Carvajal, J. *Abstracts of the Satellite Meeting on Powder Diffraction of the XV Congress of the IUCr* **1990**, 127.
(14) De Grave, E.; Vandenberghe, R. E.; Dauwe, C. *Hyperfine Interact.* **2005**, *161*, 147.
(15) Gauthier, C.; Sole, V. A.; Signorato, R.; Goulon, J.; Moguiline, E. *J. Synchrot. Radiat.* **1999**, *6*, 164.
(16) Solé, V. A.; Gauthier, C.; Goulon, J.; Natali, F. *J. Synchrot. Radiat.* **1999**, *6*, 174.
(17) Wilke, M.; Farges, F.; Petit, P. E., Jr.; Martin, F. *Am. Mineral.* **2001**, *86*, 714.
(18) Giuli, G.; Paris, E.; Pratesi, G.; Koeberl, C.; Cipriani, C. *Meteorit. Planet. Sci.* **2003**, *38*, 1181.
(19) Da Costa, G. M.; Van San, E.; De Grave, E.; Vandenberghe, R. E.; Barrón, V.; Datas, L. *Phys. Chem. Miner.* **2002**, *29*, 122.
(20) Ericson, T.; Wappling, R. *J. Phys. (Paris)* **1976**, *37*, C6–719.
(21) Greneche, J. M.; Varret, F. *J. Phys. Lett.* **1998**, *43*, L233.
(22) Bødker, F.; Mørup, S.; Linderoth, S. *Phys. Rev. Lett.* **1994**, *72*, 282.
(23) Farges, F. *Phys. Chem. Miner.* **2001**, *28*, 619.
(24) Giuli, G.; Eeckhout, S. G.; Paris, E.; Koeberl, C.; Pratesi, G. *Meteorit. Planet. Sci.* **2005**, *40*, 1575.
(25) Westre, T. E.; Kennepohl, P.; DeWitt, J. G.; Hedman, B.; Hodgson, K. O.; Solomon, E. I. *J. Am. Ceram. Soc.* **1997**, *119*, 6297.
(26) Glatzel, P.; Mirone, A.; Eeckhout, S. G.; Sikora, M.; Giuli, G. *Phys. Rev. B* **2008**, *77*, 1.
(27) Laurent, Ch.; Blaszczyk, Ch.; Brieu, M.; Rousset, A. *Nanostruct. Mater.* **1995**, *6*, 317.
(28) Laurent, Ch.; Peigney, A.; Rousset, A. *J. Mater. Chem.* **1998**, *8*, 1263.

JP8032098